Biomed Microdevices (2016) 18:61
DOI 10.1007/s10544-016-0092-9

Improved synthesis and growth of graphene oxide for field effect transistor biosensors

Jingfeng Huang[1,2,3] · **Hu Chen**[1,2] · **Lin Jing**[1,2] · **Derrick Fam**[4] · **Alfred Iing Yoong Tok**[1]

Abstract Reduced graphene oxide (RGO) has many advantages over graphene such as low-cost, aqueous processable and industrial-scalable. However, two main limitations that prevent the use of RGO in electronics are the high electrical resistance and large electrical resistance deviation between fabricated devices. This limits RGO's use in biosensors, capacitors and other electronic devices. Herein, we present (1) a modified Hummer's method to obtain large RGO flakes via in-situ size fractionation and (2) the novel growth of RGO which can bridge the gaps in-between existing RGO flakes. Together, these two processes reduced the electrical resistance drastically from 1.99E + 06 to 4.68E + 03 Ω/square and the standard deviation decreased from 80.5 % to 16.5 %. The RGO was then fabricated into a field-effect transistor biosensor. A 1 pmol to 100 nmol change in Cytochrome C protein corresponded to a 3 % change in electrical resistance. The reported improved RGO synthesis method and subsequent growth enable large-scale application of RGO in practical electronic devices such as biosensors.

Keywords Large graphene oxide flake · Chemical derived graphene flake, 2-dimensional material · Carbon material · Biological sensor transducer · Chemical vapour deposition

1 Introduction

Graphene, a single-atom-thick and two-dimensional carbon nanomaterial, had attracted increasing attention in various applications such as field-effect transistors (Xia et al. 2010; Kim et al. 2009a; Chen et al. 2016a; Chen et al. 2016b; Chen et al. 2016c; Huang et al. 2015; Chen et al. 2015). However, the zero band-gap in the material limits its potential in biosensors. Alternatively, reduced graphene oxide (RGO), also known as chemically derived graphene (CDG) or functionalized graphene nanosheets (FGS), has a natural band-gap, can be scaled up and further functionalised easily (Li et al. 2009a; Teng et al. 2012). RGO can be used as an alternative to graphene and other carbon derivatives in electronics because it is single-atom-thick and has a tunable band gap with the advantage of a scalable solution processable route (Jing et al. 2016; Stankovich et al. 2007; Dreyer et al. 2010; Loh et al. 2010; Eda et al. 2008; Gunho et al. 2010; Kim et al. 2009b).

However, current RGO devices have high resistance and high variation in its electrical resistivity. Prior applications, such as for transparent conductors (Becerril et al. 2008) and field effect transistors (Jung et al. 2008) were limited to individual graphene oxide sheets. This is due to the varying coverage of RGO flakes that ranges from 60 to 90 %. For this

✉ Alfred Iing Yoong Tok
miytok@ntu.edu.sg

[1] School of Materials Science and Engineering, Nanyang Technological University, Singapore 639798, Singapore

[2] Institute for Sports Research, Nanyang Technological University, 50 Nanyang Avenue, Singapore 639798, Singapore

[3] School of Engineering, Republic Polytechnic, 9 Woodlands Ave 9, Singapore 738984, Singapore

[4] Department of Chemistry, Royal College of Science, Imperial College, Exhibition Road, London SW72AZ, UK

Published online: 05 July 2016

reason, large-sized and 100 % coverage like chemical vapour deposition (CVD) grown graphene (Li et al. 2009a; Gunho et al. 2010; Kim et al. 2009b; Li et al. 2009b) is necessary to homogenize the RGO coverage. In this paper, we report a modified Hummer's method with *in-situ* size fractionation to obtain large-sized GO flakes and subsequently, a post-treatment process to extend the RGO coverage to 100 %.

In this paper, through a systematic manner, the role and mechanism of pre-oxidation and *in-situ* size fractionation in modified Hummer's method are elucidated. This study allows large mono-layered graphene oxide to be obtained, and is subsequently used for subsequent growth of RGO to obtain a highly-conductive and highly-electrical homogenous transducer suitable for field effect transistor biosensors.

2 Methods

2.1 Synthesis of large GO flakes

An improved modified Hummers method (Larisika et al. 2012; Su et al. 2009; Huang et al. 2016; Huang et al. 2014a) was used to obtain large Graphene Oxide (GO) sheets. Concisely, 2 g of 3–5 mm graphite flakes (NGS, Leinburg, Germany) were mixed with H_2SO_4 (12 ml) for 4 h at 80 °C and placed in an ultra-sonication bath for 1 h. The flakes were then diluted. The diluted flakes were then washed with DI water over a 0.4 μm nylon filter and dried overnight.

For the drying process, three conditions were tested out - under ambient drying (not as practical as the drying process is long), mild heating (70 °C) and vacuum desiccator. A drop of GO solution (from the same batch) was dropped onto SiO_2 chip and each chip was dried under different conditions for 24 h. For mild heating, the chip was placed on a heater plate with temperature controlled at 70 °C. All three samples were kept away from the light during the process. GO dried under these conditions were then characterized using the water contact angle measurement.

To obtain the yield difference from this drying process, the oven-dried and the vacuum-dried GO were oxidised. They were then subsequently exfoliated and centrifuged at 5000G for 3 min to obtain the GO solution. 1 ml of GO solution from oven-dried and vacuum-dried were placed in 2 Eppendorf tubes each and freeze-dried. The yield concentration of the GO is obtained via the weight difference between the empty tube weight and the tube after freeze drying. We hypothesized that the drying condition could affect the final yield of GO.

The pre-oxidized graphite powder were then added to H_2SO_4 (120 ml) and $KMnO_4$ (15 g) and stirred for 2 h. DI water (250 ml) was then slowly added to the mixture in an ice bath and stirred for another 2 h. Thereafter, DI water (700 ml) and H_2O_2 (20 ml) was added to stop the reaction.

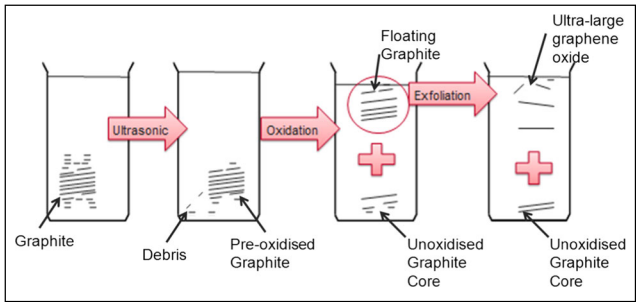

Fig. 1 Schematic of improved GO synthesis. The reported method adds the ultrasonication, the vacuum-drying and the selective exfoliation steps to obtain large-sized GO suitable for subsequent post-treatment

The addition of concentrated sulphuric acid (H_2SO_4) to potassium permanganate ($KMnO_4$) is a potentially explosive oxidation step. The reaction between sulphuric acid and potassium permanganate form reactive dimanganese-heptoxide, which is known to detonate when heated to above 55 °C. Subsequent addition of hydrogen peroxide (H_2O_2) reduces potassium permanganate to manganese sulphate and this stops the oxidation process.

After the main oxidation step, two distinct layers were obtained – floating graphite layer and the debris layer. The floating layer were removed and transferred to a new container with 1 l of DI water for physical exfoliation at 200 rpm (48 h) using a magnetic stirrer. Subsequently, the mixture was centrifuged at 5000G for 3 min. The centrifuged solution separated into 3 distinct portions.

Different portions of the solution were used for the fabrication of GO on SiO_2 to obtain how the different portion of the GO solution will affect the final fabrication of GO on SiO_2. Silicon dioxide (SiO_2) substrates were RCA cleaned 2 times and then functionalized in 1 % (*v*/v) 3-APTES ethanol solution for 1 h. The different portions of the GO solution was then drop-casted on the substrates and left to react for 1 h. The substrates were subsequently rinsed and kept under ambient conditions. SEM (JEOL-7600F, 1KeV with gentle beam) was used to analyse the GO on the SiO_2 substrate. We hypothesize that different portions of the GO solution will yield different characteristic that are suitable for different applications.

2.2 Growth of GO on substrate

Silicon dioxide (SiO_2) substrates were RCA cleaned 2 times and then functionalized in 1 % (*v*/v) 3-APTES ethanol solution for 1 h. Stock GO solution was then drop-casted on the

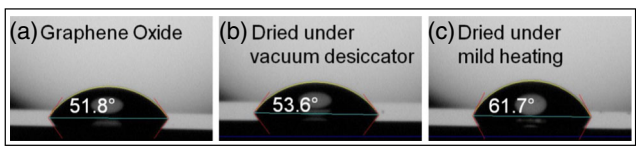

Fig. 2 Water Contact Angle measurement for **a** Graphene oxide, **b** GO dried under vacuum desiccator and **c** GO dried under mild heating

substrates and left to react for 1 h. The substrates were subsequently rinsed and kept under ambient conditions.

2.3 Ethanol CVD growth of GO

The quartz tube of the CVD was first purged with argon for 30 min. Then, prepared substrates were placed into the quartz tube of an ethanol CVD setup per batch. The temperature ramp was set at 40 °C per minute and the final temperature at 950 °C. The hydrogen and argon gas were set at 20 and 100 sccm respectively. These parameters were the optimized conditions to produce carbon nanotubes in ethanol CVD setup (Palaniappan et al. 2010).

3 Results and discussion

3.1 Modified Hummer's method with *In-situ* size fractionation

Although pre-oxidation steps had been commonly used in synthesis of aqueous graphene, the role and mechanism of pre-oxidation on graphite had yet been determined. For smaller graphite flakes (micron-sized), a chemical pre-oxidation was used to obtain a higher yield of GO from micron-sized graphite (Xu et al. 2008). Then in 2009, Su et al. (Su et al. 2009) used ultra-sonication on large graphite flakes (3-5 mm across) to substitute the chemical pre-oxidation step and this resulted in large flakes (up to 3 mm) with higher mobility values up to 12cm^2/Vs. Adding a ultra-sonication pre-oxidation step to the Hummer's method, was reported to enlarge the size of aqueous graphene (Su et al. 2009; Kovtyukhova et al. 1999). With larger flakes, the carrier mobility and the electrical conductivity (Kholmanov et al. 2012) could be increased while maintaining high optical transparencies (Larisika et al. 2012).

Ultra-sonication was used as a pre-oxidation step (Fig. 1). After ultra-sonication, small graphite debris was broken off from the graphite cores. The weight and average size (Dynamic Light Scattering) of the debris removed were 0.57 g and 6.79 μm respectively. As the maximum size of aqueous graphene obtained was limited to the largest size of graphene domains in the graphite flake from which it was chemically synthesized (Eda and Chhowalla 2010), the broken down debris were removed via filtration.

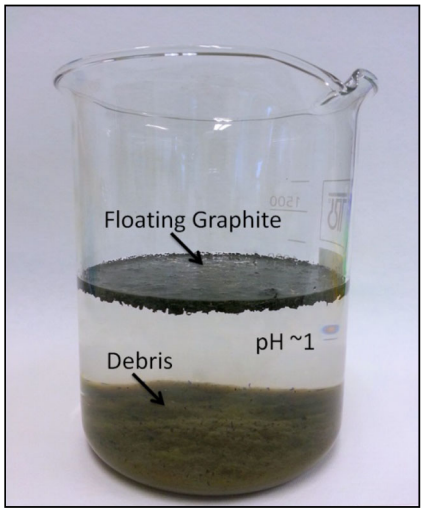

Fig. 3 After main oxidation step, two distinct layers were obtained – floating graphite layer and the debris layer

The pre-oxidised graphite was then dried in a vacuum desiccator before being oxidised with the strong oxidising agents. Literatures (Su et al. 2009; Hou et al. 2010; Luo et al. 2012) had reportedly used mild heat to dry the pre-oxidised GO at this stage. It was detrimental to the GO and it reduces the GO permanently. Even usage of mild heating at 70 °C reduced the GO. This reduction could be measured using the water contact angle measurement shown in Fig. 2. Drying under mild heating (70 °C) increased the contact angle by ~10° from 51.8°, whereas vacuum desiccator sample only increased by 1.8°. Although the GO after drying in vacuum desiccator was not fully removed of water (Malhotra et al. 2010), but it was safe for reaction with the concentrated acid in subsequent step.

From Table 1, the final GO yield concentration difference between oven and vacuum dried sample was significant. The concentration obtained from the oven-dried samples was 2.9 times less than the vacuum-dried. Thus, from the contact angle measurement and the GO concentration measurements, oven-drying was detrimental to the yield of GO synthesis.

In contrast to using ultra-sonication method for exfoliation (Eda et al. 2008; Park and Ruoff 2009), after the pre-oxidation our method do not use ultra-sonication that could break up large GO to result in smaller GO sheets, A mixture of floating

Table 1 Comparison of GO yield concentration between oven-dried and vacuum-dried pre-oxidised samples (the GO solution was obtained after centrifuging at 5000G for 3mins)

Freeze Dried Samples	Samples	Empty Tubes (mg)	Final Weight (mg)	Conc. (mg/ml)	Average Conc. (mg/ml)	Standard Deviation
Oven-dried	A	993.23	993.48	0.25	0.1950	0.08
	B	1005.17	1005.31	0.14		
Vacuum-dried	A	985.91	986.45	0.54	0.5650	0.04
	B	996.22	996.81	0.59		

graphite flakes and sunken graphite flakes was obtained after synthesis (Fig. 3). Some graphite flakes floated because larger GO sheets were adhered to the graphite core and these larger GO sheets prefer the air-water interface due to size dependent amphiphilicity of GO.

The floating flakes were removed from the original mixture and transferred to a new container with fresh DI water for subsequent exfoliation. The exfoliation of the aqueous graphene from the graphite core was carried out by mild stirring in DI water. The mechanical movement helped the large graphene oxide flakes that were all weakly adhered to the core peel off. The higher pH value also helped with the effective exfoliation. This pH-dependent exfoliation behaviour of graphene-oxide aqueous solution could be due to the deprotonate of carboxyl groups in the GO sheets thus becoming more hydrophilic and dissolves into the bulk aqueous solution (Shih et al. 2012; Bai et al. 2011).

Dynamic mechanical analyser (TA Instruments, DMA Q800) was used to obtain the force needed to fully delaminate the top layer of GO and graphene from the oxidised graphite core and graphite core respectively. Vacuum-dried GO and graphite were fixed (2 N force) using heat-releasing tape to the holders of the DMA. The maximum force required to delaminate the material was recorded. 30 samples of graphite and GO each were measured.

The average forces needed for the graphite and GO were 0.330 N and 0.012 N respectively. The force needed to delaminate GO was ~30 times smaller than that of graphite. A gentle exfoliation step after the oxidation by the mechanical stirrer was sufficient to separate the GO from the oxidised graphite core.

The physical transferring of the GO flakes into another container of DI water for exfoliation increased the effectiveness of GO exfoliation. The exfoliation of GO was improved at pH of 7 compared to a more acidic pH. This is could be due to the presence of carboxyl groups that decreased the net energetic cost or enthalpy of mixing (Hernandez et al. 2008) which increased the interaction between solvent and the GO basal planes. To confirm if neutral pH is better for exfoliation, the un-exfoliated floating flake was membrane-dialysed using 3000 Molecular Weight Cut-Off (MWCO) membranes before centrifugation. Then the membrane was sealed and placed in a large reservoir of DI water under stirring. The result was tabulated in Table 2 where the average concentration of membrane-dialysed GO was increased 2.3 times, from 0.5650 to 1.2950 mg/ml. The increased GO yield obtained for GO exfoliation at higher pH showed that neutral pH was advantageous to exfoliation.

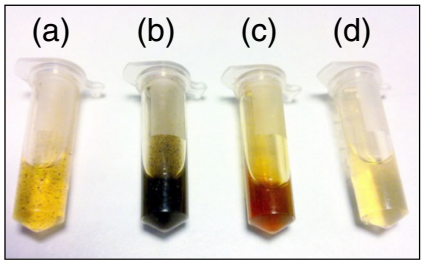

Fig. 4 **a** Mixture after mechanical stirring of the large floating GO flakes, before centrifugation. After centrifugation, the solution shows 3 distinct portions **b** lower graphite portion with un-oxidised graphite, **c** middle portion with some un-oxidised graphite and **d** upper portion with GO flakes

Figure 4a shows the mixture after this mechanical exfoliation. After centrifugation, three distinct portions were obtained – a lower graphite portion with un-oxidised graphite (Fig. 4b), middle portion with some un-oxidised graphite (Fig. 4c) and upper portion with completely exfoliated GO flakes (Fig. 4d).

Different portions obtained from the GO mixture were used for the fabrication of GO on SiO_2 substrates. The fabricated GO on SiO_2 substrates from the top portion (Fig. 5a) of the GO synthesis mixture after centrifugation was generally well-covered with large GO flakes besides some gaps. The GO on SiO_2 substrates fabricated from the middle portion (Fig. 5b) showed multi-layered GO sheets which were not completely exfoliated, while the lower portion (Fig. 5c) showed unreacted graphite. Both the middle and lower portions of the GO synthesis mixture are thus not suitable for applications that required single layer of GO, but suitable for electronic connectors which do not require single layer GO.

Figure 6 shows a typical tapping mode AFM image of GO deposited on a silica substrate by drop-casting method. The thicknesses of monolayer GO flakes were typically in the range of 0.7-1 nm (Stankovich et al. 2007; Marcano et al. 2010; Gao et al. 2010; Gilje et al. 2007). From the AFM height profile it was shown that the thickness for the GO sheet

Table 2 Exfoliated GO concentration obtained after the samples were exfoliated at different pH

Freeze Dried Samples	Samples	Empty Tubes (mg)	Final Weight (mg)	Conc. (mg/ml)	Average Conc. (mg/ml)
Vacuum-dried, exfoliated at ~pH 1	A	985.91	986.45	0.54	0.5650
	B	996.22	996.81	0.59	
Vacuum-dried, exfoliated at ~pH 7	A	1037.41	1038.72	1.31	1.2950
	B	1037.82	1039.1	1.28	

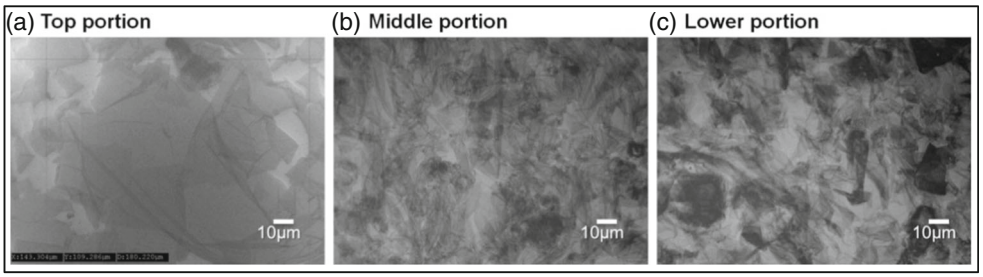

Fig. 5 SEM images of GO flakes on SiO_2 from the **a** top **b** middle and **c** lower portion part of the GO synthesis mixture after centrifugation

obtained by the reported modified method was ~1 nm, corresponding to a single layer of GO.

The scanning electron microscopy (SEM) image of an ultra-large hydrazine vapour reduced GO flake, which was approximately 60 μm in lateral size deposited on SiO_2/Si substrate, was shown in Fig. 7a. Smaller GO fragments were also observed beside the ultra-large flakes. About 1000 GO flakes were measured and the corresponding size histogram is illustrated in Fig. 7b. The average size of the GO flakes obtained by the improved synthesis was 700 μm^2, hence the GO flakes were ~7 times larger in area than those produced using previously reported method (Luo et al. 2009).

Thus the reported improved modified Hummer's method was able to synthesize larger GO flakes with a combination of (1) vacuum-drying process, (2) selective fractionation of floating flakes and (3) neutral pH exfoliation methods. These large GO flakes were used as the template for the subsequent growth of RGOs for homogenous transducer suitable for FET sensors.

3.2 Growth of reduced graphene oxide for homogenous biosensor transducers

To grow graphene, a catalyst such as copper (Li et al. 2009b) or nickel (Kim et al. 2009c) is needed. The high carbon solubility of nickel film allows the diffusion of carbon into the film at growth temperature and precipitate out of the substrate upon cooling; whereas the low carbon solubility of copper catalytically decomposes alcohol into radicals and allows precipitation of the carbon on the surface (Li et al. 2009a).

Recently, the extended growth of carbon nanotube without any additional catalyst has been reported (Yao et al. 2009). The extended growth followed the configuration and structure of the original nanotube template. A convincing model is still lacking on how the carbon is nucleated and grown from this template. There had been reports of using ethanol CVD to repair both graphene and GO (Gong et al. 2012; Su et al. 2010); but no growth was observed. Herein, our group proposes a hypothesis that extended growth of GO by ethanol CVD is possible.

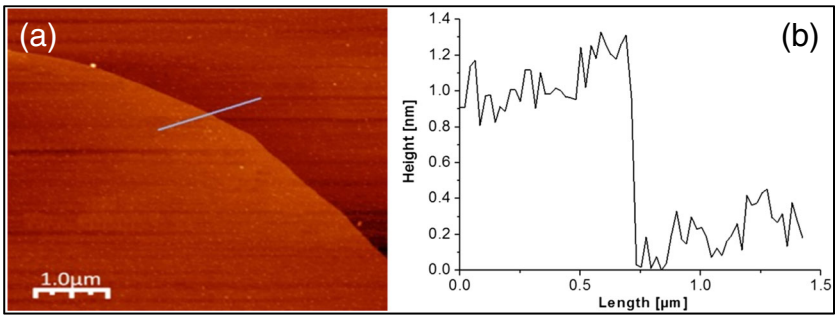

Fig. 6 **a** AFM image of GO and **b** AFM height profile for the GO sheet

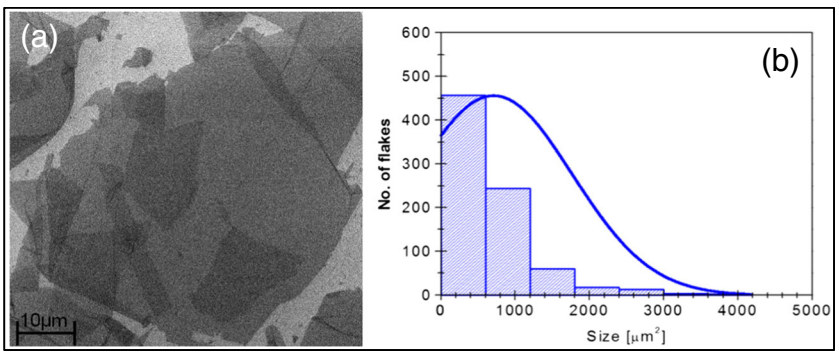

Fig. 7 **a** SEM image of a large GO sheet on SiO_2 substrate produced from the improved modified Hummer's method. **b** Size distribution of GO flakes

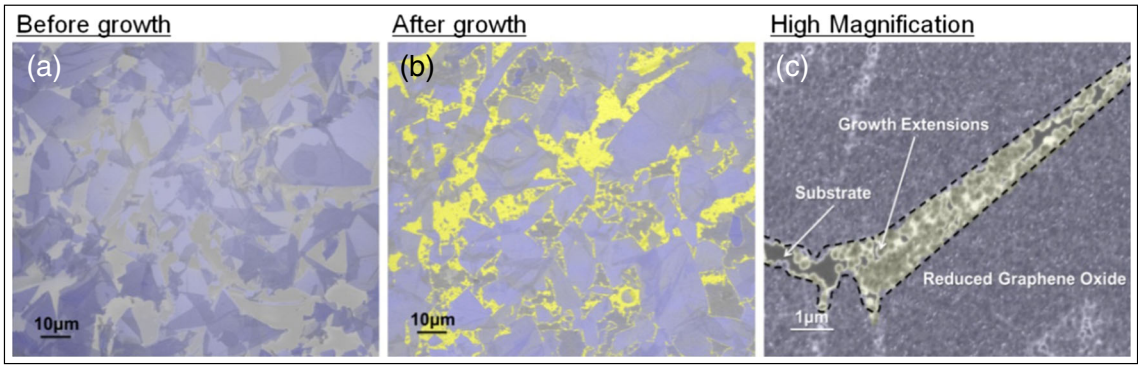

Fig. 8 SEM image of **a** GO flakes, **b** RGO flakes after ethanol CVD treatment of 1 h and **c** the high magnification of the new growth. The GO coverage increased from 65 % to 80 %. The GO flakes are highlighted in purple and the growth in yellow. SiO_2 substrate is grey in colour

The SEM images of the GO flakes before (Fig. 8a), after a partial ethanol (Fig. 8b) CVD growth and the high magnification of the new growth (Fig. 8c) are shown. The additional GO new growth were observed to be lighter in shade compared to pre-existing flakes. The contrast mechanism was due to e-beam-induced surface potential between graphene of different band gaps (Li et al. 2012). ImageJ software was used to obtain the coverage area of GO and the new coverage areas on the SEM images. After an ethanol CVD treatment of 1 h, the GO coverage increased from 65 % to 80 %. The high magnification image shows the new growth islets between the gaps of two flakes. The ethanol precursor provides the carbon radicals for deposition (Eq. 1); in direct competition with the hydrogen in the gas precursor which etches away amorphous carbon thus allowing controlled monolayer growth. The competition between these two precursors can be written in the form of the Le Chatelier's equation (Eq. 2).

$$C_xH_y\ (g) \leftrightarrow x\ C\ (s) + (y/2)\ H_2\ (g) \quad (1)$$

$$C\ (s) + 2\ H_2\ (g) \rightarrow CH_4\ (g) \quad (2)$$

From Fig. 9, as the ethanol CVD treatment time proceeds up to the first hour, both the height of the original GO and new growth increases. Height peaks begin to appear in the first hour. In the second hour, only the new growth continue to increase and it eventually forms a continuous layer with 2 nm thickness, corresponding to ~2 layers of GO (Huang et al. 2013a).

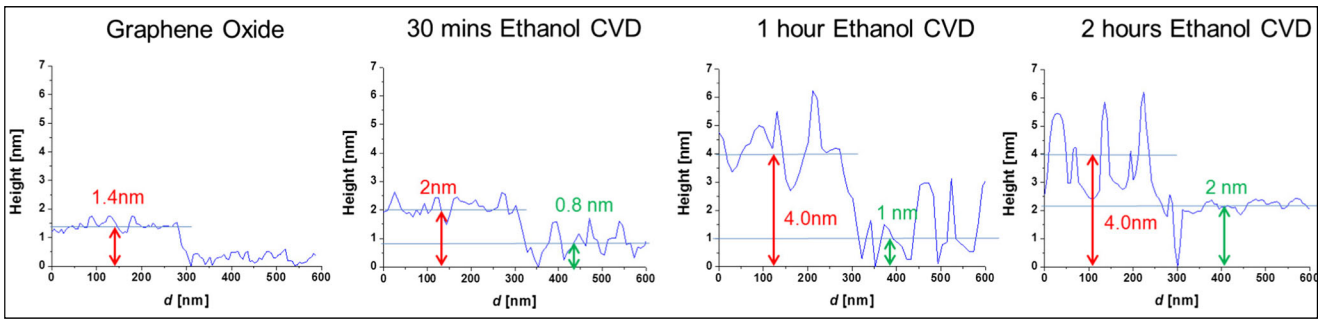

Fig. 9 AFM height profile and corresponding height of GO at different stages of ethanol CVD

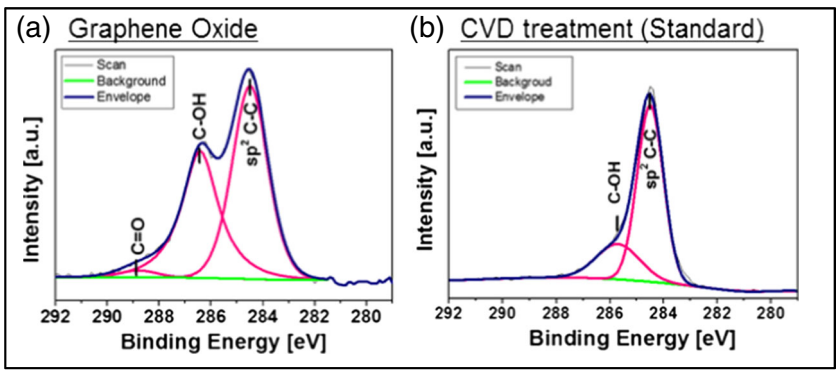

Fig. 10 C1s XPS spectra (hv = 1486.6 eV) collected on **a** GO; and Reduced GO reduced in similar CVD setup with **b** 1 h ethanol CVD treatment

Table 3 Atomic percentage of different carbon bonds identified by XPS on a sample of mono-layered GO and a sample of CVD reduced GO

Samples	C = O (atomic %)	C-OH (atomic %)	C-C (atomic %)
GO	2.4	38.7	58.9
CVD Reduced GO	0	17.2	82.8

The C1s spectral of rGO shown in Fig. 10 was deconvoluted using Lorentzian with Gaussian broadening curve-fitting into C = O (~287.2 eV), C-OH (~286.3 eV) and C-C (284.5 eV). These values were in agreement with previous reports (Su et al. 2009; Huang et al. 2013a; Yang et al. 2009). The C-C spectra positions for both samples were detected to be at 284.5 eV.

As shown in Fig. 10, the ethanol CVD treated sample had both C = O and C-OH down-shifted. This showed that the presence of hydrogen gas in the ethanol system acted as an etchant which could anisotropically etch amorphous carbon to produce reduced GO closer to that of HOPG, similar to what had been reported for graphene systems (Zhang et al. 2011). Hydrogen also preferentially etch away stacked carbon (16 kJ/mol) and some oxygen moieties due to the weaker bond compared to in-plane carbon (345 J/mol) thus leading to more graphitized rGO instead of amorphous carbon (Yuan et al. 2009). The atomic percentages of the bonds present in the XPS spectra was then calculated and presented in Table 3.

Table 3 shows that for the sample with ethanol CVD treatment, the C = O bond peak (initially at 2.4 %) was completely removed indicating an efficient graphitization. The C = O bond in the CVD treatment had been reduced to C-OH and C-C (Huang et al. 2013a).

The effect of CVD process time on the electrical resistance on the samples using a 4-point probe setup was also investigated. Table 4 shows that average sheet resistance of RGO decreased 3 orders of magnitude from 1.99E + 06 (12 h hydrazine) to 4.68E + 03 (2 h ethanol CVD) Ω/□. The corresponding relative standard deviation also decreased from 80.5 % to 16.5 %. The decrease in electrical resistivity could be due to the increased percolation pathways between flakes from the new growths. The ethanol CVD treatment decreased the standard deviation of inter-measurement sites significantly, thus solving a critical problem for the practical use of RGO in electronics such as the development of biosensors (Faulkner et al. 2014; Huang et al. 2013b; Huang et al. 2013c) and microelectronics (Su et al. 2009; Huang et al. 2014b).

Figure 11 shows a schematic of a field-effect-transistor (FET) biological sensor platform that could be fabricated on top of the post-treated GO transducer reported in earlier sections. Gold electrodes are deposited on the transducer. Then, a silicone rubber well is fixed on the electrodes. The liquid analyte of interest can then be placed into the silicone well and interact with the transducer. Different liquid analyte will interact differently with the transducer and result in different FET behaviour. This behaviour can be recorded in a semiconductor parametric analyser. The signatures can be used to identify and quantify the liquid analyte.

FET platform can be used for the (Xia et al. 2010) study of the conduction mechanism, (Kim et al. 2009a) optimization of the growth time, and (Chen et al. 2016a) the application of the post-treated RGO to sensing of molecules (Fam et al. 2011) such as Interleukin-6 bio-molecule (Leggate et al. 2010; Gray et al. 2009) and hydrogen sulphide gas (Fam et al. 2009).

A three electrode system was applied to the fabricated field effect transistor platform – source, drain and gate electrode, using a semiconductor parametric analyser (Keithley, 4200-SCS). Gate voltage applied via the electrolyte, shifts the post-treated GO Fermi layer and results in a conductance change. In Fig. 12a, when the Fermi level crosses over the Dirac point(V_d), the majority charge carrier is changed and lead to ambi-polar behavior (Hess et al. 2011). Two transport regimes are observed on both sides of the Dirac point, the hole ($V_g < V_d$) and electron ($V_g > V_d$) regime. The transconductance or the slope of the I_d vs. V_g graph shows that the hole regime is higher. Thus transport in hole regime will have a higher current response to a small modulation of the gate voltage and thus the sensitivity. The minimum current, which is the Dirac point, is observed at V_d = +230 mV. This shift in Dirac point is due to substrate-induced doping. The leakage current levels of the device chip were negligible (3 magnitudes lower) compared to the I_d.

This set-up was used to test for Cytochrome C, a readily available protein. PBSE-Cytochrome C was used for the antibody-antigen binding. It was observed that the sensing window is from 1pM to 100 nM(Fig. 12b). The chip is

Table 4 Four-point probe sheet resistance for GO reduced under different conditions (n = 5)

Reduction Method	Hydrazine vapour	Ethanol CVD			
Processing Time Average	12 h	15 mins	30 mins	1 h	2 h
Resistance (Ω/□)	1.99E + 06	6.10E + 04	2.87E + 04	2.23E + 04	4.68E + 03
Relative Standard Deviation (%)	80.5	72.6	43.6	32.1	16.5

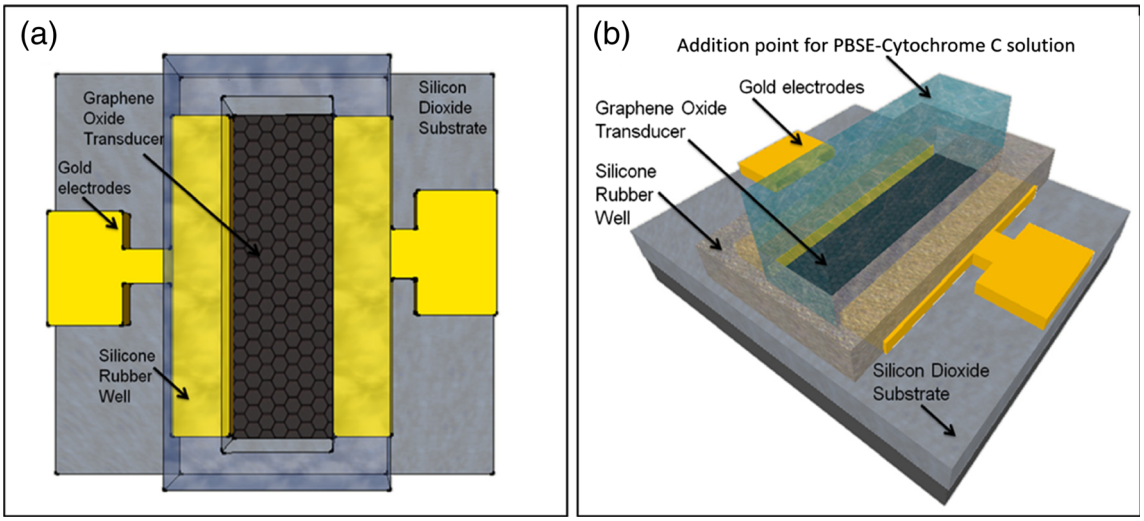

Fig. 11 Schematic showing **a** top-view and **b** side-view of fabricated FET devices with silicone well suitable for analyte testing

exposed to different concentrations of proteins and due to the antigen-protein interaction or doping effect, there is a change in conductance/mobility and this electrical change is measured by a parametric analyser station.

The Cytochrome C Isoelectric Point is 10. Therefore at pH 7.4 (test condition), Cytochrome C is positively charged. Conductance of hole decreases as more Cytochrome C is attached onto transducer. Sensing window from 1 pmol to 100 nmol of Cytochrome C (3 % change in conductance). The chip is stable up to 4 h in buffer solution without optimization.

4 Conclusions

In summary, it was shown that large GO flakes could be obtained using the improved modified Hummer's method, due to (1) larger graphite precursor, (2) physical size fractionation and (3) neutral pH exfoliation. These large GO flakes were used as the template for the subsequent growth of RGO flakes for homogenous transducer suitable for FET sensors. The lateral size of GO could be grown up to 100 % coverage on silicon substrate (from ~60–85 %). The growth reduced both the variable coverage and the electrical resistance deviation between chips (80.5 % to 16.5 %). In tandem, the improved synthesis of GO and growth of GO technologies could enable large-scale application of RGO to be used in practical electronic devices such as biosensors. In virtue of the signal enhancement effect by the post-treated graphene, the developed FET sensor responded to pM levels of target molecules. A 1 pmol to 100 nmol change in Cytochrome C protein corresponded to a 3 % change in electrical resistance.

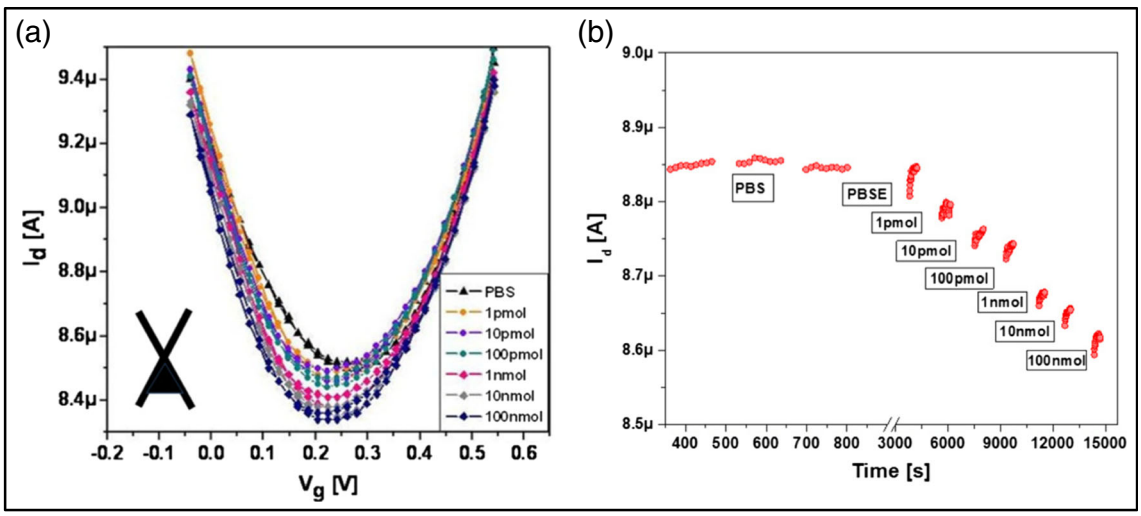

Fig. 12 **a** Concentration dependent response of Cyctrochrome C to drain current. Insert shows the position of the Fermi level **b** Detection of different Cytochrome C concentrations on rGO device at gate voltage (Vg) = +100 mV

Acknowledgments The research was funded by the Institute for Sports Research (ISR) of Nanyang Technological University (NTU). The research was also partly supported by NTU-HUJ-BGU Nanomaterials for Energy and Water Management Programme under the Campus for Research Excellence and Technological Enterprise (CREATE), that is supported by the National Research Foundation, Prime Minister's Office, Singapore. The author would like to thank Dr. Alagappan Palaniappan from NTU's Centre for Biomimetic Sensor Science (CBSS) for aiding with the ethanol CVD setup.

References

H. Bai, C. Li, X. Wang, G. Shi, J. Phys. Chem. C **115**, 5545–5551 (2011)

H. A. Becerril, J. Mao, Z. Liu, R. M. Stoltenberg, Z. Bao, Y. Chen, ACS Nano **2**, 463–470 (2008)

H. Chen, S. K. Lim, P. Chen, J. Huang, Y. Wang, A. Palaniappan, M. Platt, B. Liedberg, A. I. Y. Tok, Phys. Chem. Chem. Phys. **17**, 3451–3456 (2015)

H. Chen, J. Huang, A. Palaniappan, Y. Wang, B. Liedberg, M. Platt, A. I. Y. Tok, Analyst **141**, 2335–2346 (2016a)

H. Chen, P. Chen, J. Huang, R. Selegård, M. Platt, A. Palaniappan, D. Aili, A. I. Y. Tok, B. Liedberg, Anal. Chem. **88**, 2994–2998 (2016b)

H. Chen, T. K. Choo, J. Huang, Y. Wang, Y. Liu, M. Platt, A. Palaniappan, B. Liedberg, A. I. Y. Tok, Mater. Des. **90**, 852–857 (2016c)

D. R. Dreyer, S. Park, C. W. Bielawski, R. S. Ruoff, Chem. Soc. Rev. **39**, 228–240 (2010)

G. Eda, M. Chhowalla, Adv. Mater. **22**, 2392–2415 (2010)

G. Eda, G. Fanchini, M. Chhowalla, Nat Nano **3**, 270–274 (2008)

D. W. H. Fam, A. I. Y. Tok, A. Palaniappan, P. Nopphawan, A. Lohani, S. G. Mhaisalkar, Sensors Actuators B Chem. **138**, 189–192 (2009)

D. W. H. Fam, A. Palaniappan, A. I. Y. Tok, B. Liedberg, S. M. Moochhala, Sensors Actuators B Chem. **157**, 1–7 (2011)

S. Faulkner, K. Spilsbury, J. Harvey, A. Jackson, J. Huang, M. Platt, A. Tok, M. Nimmo, Eur. J. Appl. Physiol., 1–10 (2014). doi:10.1007/s00421-014-2851-8,

L. Gao, J. R. Guest, N. P. Guisinger, Nano Lett. **10**, 3512–3516 (2010)

S. Gilje, S. Han, M. Wang, K. L. Wang, R. B. Kaner, Nano Lett. **7**, 3394–3398 (2007)

C. Gong, M. Acik, R. M. Abolfath, Y. Chabal, K. Cho, J. Phys. Chem. C **116**, 9969–9979 (2012)

S. R. Gray, M. Clifford, R. Lancaster, M. Leggate, M. Davies and M. A. Nimmo, Cytokine, 2009, 47, 98–102.

J. Gunho, C. Minhyeok, C. Chu-Young, K. Jin Ho, P. Woojin, L. Sangchul, H. Woong-Ki, K. Tae-Wook, P. Seong-Ju, H. Byung Hee, K. Yung Ho, L. Takhee, Nanotechnology **21**, 175201 (2010)

Y. Hernandez, V. Nicolosi, M. Lotya, F. M. Blighe, Z. Sun, S. De, I. T. McGovern, B. Holland, M. Byrne, Y. K. Gun'Ko, J. J. Boland, P. Niraj, G. Duesberg, S. Krishnamurthy, R. Goodhue, J. Hutchison, V. Scardaci, A. C. Ferrari, J. N. Coleman, Nat. Nanotechnol. **3**, 563–568 (2008)

L. H. Hess, M. Jansen, V. Maybeck, M. V. Hauf, M. Seifert, M. Stutzmann, I. D. Sharp, A. Offenhäusser, J. A. Garrido, Adv. Mater. **23**, 5045–5049 (2011)

S. Hou, S. Su, M. L. Kasner, P. Shah, K. Patel, C. J. Madarang, Chem. Phys. Lett. **501**, 68–74 (2010)

J. Huang, M. Larisika, W. H. D. Fam, Q. He, M. A. Nimmo, C. Nowak, I. Y. A. Tok, Nanoscale **5**, 2945–2951 (2013a)

J. Huang, J. Harvey, H. Chen, M. A. Nimmo and I. Y. A. Tok, Vilamoura, Portugal, 2013b.

J. Huang, J. Harvey, W. H. D. Fam, M. A. Nimmo, I. Y. A. Tok, Procedia Engineering **60**, 195–200 (2013c)

J. Huang, J. Harvey, H. Chen, W. H. D. Fam, M. A. Nimmo and I. Y. A. Tok, Chinese Physics B, 2014a.

J. Huang, D. Fam, Q. He, H. Chen, D. Zhan, S. H. Faulkner, M. A. Nimmo, A. I. Yoong Tok, J. Mater. Chem. C **2**, 109–114 (2014b)

J. Huang, H. Chen, W. Niu, D. W. H. Fam, A. Palaniappan, M. Larisika, S. H. Faulkner, C. Nowak, M. A. Nimmo, B. Liedberg and A. I. Y. Tok, RSC Advances, 2015, 5, 39245–39251.

J. Huang, M. Larisika, C. Nowak and I. Y. A. Tok, New Methods in Aqueous Graphene (Graphene Oxide) Synthesis for Biosensor Devices, Taylor & Francis Group, 2016, Submitted.

L. Jing, R. Y. Tay, H. Li, S. H. Tsang, J. Huang, D. Tan, B. Zhang, E. H. T. Teo, A. I. Y. Tok, Nanoscale **8**, 11114–11122 (2016)

I. Jung, D. A. Dikin, R. D. Piner, R. S. Ruoff, Nano Lett. **8**, 4283–4287 (2008)

I. N. Kholmanov, M. D. Stoller, J. Edgeworth, W. H. Lee, H. Li, J. Lee, C. Barnhart, J. R. Potts, R. Piner, D. Akinwande, J. E. Barrick, R. S. Ruoff, ACS Nano **6**, 5157–5163 (2012)

S. Kim, J. Nah, I. Jo, D. Shahrjerdi, L. Colombo, Z. Yao, E. Tutuc, S. K. Banerjee, Appl. Phys. Lett. **94**, 062107 (2009a)

K. S. Kim, Y. Zhao, H. Jang, S. Y. Lee, J. M. Kim, K. S. Kim, J.-H. Ahn, P. Kim, J.-Y. Choi, B. H. Hong, Nature **457**, 706–710 (2009b)

K. S. Kim, Y. Zhao, H. Jang, S. Y. Lee, J. M. Kim, K. S. Kim, J. H. Ahn, P. Kim, J. Y. Choi, B. H. Hong, Nature **457**, 706–710 (2009c)

N. I. Kovtyukhova, P. J. Ollivier, B. R. Martin, T. E. Mallouk, S. A. Chizhik, E. V. Buzaneva, A. D. Gorchinskiy, Chem. Mater. **11**, 771–778 (1999)

M. Larisika, J. Huang, A. Tok, W. Knoll, C. Nowak, Mater. Chem. Phys. **136**, 304–308 (2012)

M. Leggate, M. A. Nowell, S. A. Jones, M. A. Nimmo, Cell Stress Chaperones **15**, 827–833 (2010)

X. Li, W. Cai, L. Colombo, R. S. Ruoff, Nano Lett. **9**, 4268–4272 (2009a)

X. Li, W. Cai, J. An, S. Kim, J. Nah, D. Yang, R. Piner, A. Velamakanni, I. Jung, E. Tutuc, S. K. Banerjee, L. Colombo and R. S. Ruoff, Science, 2009b, 324, 1312–1314.

J. Li, Y. He, Y. Han, K. Liu, J. Wang, Q. Li, S. Fan, K. Jiang, Nano Lett. **12**, 4095–4101 (2012)

K. P. Loh, Q. Bao, G. Eda, M. Chhowalla, Nat. Chem. **2**, 1015–1024 (2010)

Z. Luo, Y. Lu, L. A. Somers, A. T. C. Johnson, J. Am. Chem. Soc. **131**, 898–899 (2009)

B. Luo, X. Yan, S. Xu, Q. Xue, Electrochim. Acta **59**, 429–434 (2012)

R. Malhotra, V. Patel, J. P. Vaqué, J. S. Gutkind, J. F. Rusling, Anal. Chem. **82**, 3118–3123 (2010)

D. C. Marcano, D. V. Kosynkin, J. M. Berlin, A. Sinitskii, Z. Sun, A. Slesarev, L. B. Alemany, W. Lu and J. M. Tour, ACS Nano, 2010, 4, 4806–4814.

A. Palaniappan, W. H. Goh, J. N. Tey, I. P. M. Wijaya, S. M. Moochhala, B. Liedberg, S. G. Mhaisalkar, Biosens. Bioelectron. **25**, 1989–1993 (2010)

S. Park, R. S. Ruoff, Nat Nano **4**, 217–224 (2009)

C.-J. Shih, S. Lin, R. Sharma, M. S. Strano, D. Blankschtein, Langmuir **28**, 235–241 (2012)

S. Stankovich, D. A. Dikin, R. D. Piner, K. A. Kohlhaas, A. Kleinhammes, Y. Jia, Y. Wu, S. T. Nguyen, R. S. Ruoff, Carbon **45**, 1558–1565 (2007)

C.-Y. Su, Y. Xu, W. Zhang, J. Zhao, X. Tang, C.-H. Tsai, L.-J. Li, Chem. Mater. **21**, 5674–5680 (2009)

C.-Y. Su, Y. Xu, W. Zhang, J. Zhao, A. Liu, X. Tang, C.-H. Tsai, Y. Huang, L.-J. Li, ACS Nano **4**, 5285–5292 (2010)

X. Teng, Y. Zhu, W. Wei, S. Wang, J. Huang, R. Naccache, W. Hu, A. I. Y. Tok, Y. Han, Q. Zhang, Q. Fan, W. Huang, J. A. Capobianco, L. Huang, J. Am. Chem. Soc. **134**, 8340–8343 (2012)

F. Xia, D. B. Farmer, Y.-m. Lin, P. Avouris, Nano Lett. **10**, 715–718 (2010)

Y. Xu, H. Bai, G. Lu, C. Li, G. Shi, J. Am. Chem. Soc. **130**, 5856–5857 (2008)

D. Yang, A. Velamakanni, G. Bozoklu, S. Park, M. Stoller, R. D. Piner, S. Stankovich, I. Jung, D. A. Field, C. A. Ventrice Jr., R. S. Ruoff, Carbon **47**, 145–152 (2009)
Y. Yao, C. Feng, J. Zhang, Z. Liu, Nano Lett. **9**, 1673–1677 (2009)
G. D. Yuan, W. J. Zhang, Y. Yang, Y. B. Tang, Y. Q. Li, J. X. Wang, X. M. Meng, Z. B. He, C. M. L. Wu, I. Bello, C. S. Lee, S. T. Lee, Chem. Phys. Lett. **467**, 361–364 (2009)
Y. Zhang, Z. Li, P. Kim, L. Zhang, C. Zhou, ACS Nano **6**, 126–132 (2011)